19th Brazilian Congress of Thermal Sciences and Engineering
November 06th-10th, 2022, Bento Gonçalves - RS - Brazil

ENC-2022-0189
NUMERICAL ANALYSIS OF WATER-OIL-AIR FLOW IN A HORIZONTAL GRAVITATIONAL SEPARATOR

Daniel Rodrigues Weller
Paulo Henrique Dias dos Santos
Rigoberto Morales
Henrique Stel
Tiago Henrique Leitão Dalcuche
Marco Germano Conte
Rafael Fabricio Alves
Federal Technological University of Paraná, Department of Mechanical Engineering, R. Dep. Heitor Alencar Furtado, 5000 - Ecoville CEP 81280-340 - Curitiba - PR – Brasil.
daniel-weller@hotmail.com
paulosantos@labcet.ufsc.br
rmorales@utfpr.edu.br
stel.henrique@gmail.com
tdalcuche@gmail.com
mg_conte@hotmail.com
rafabricio@live.com

Abstract. *Gravitational separators are large equipment, which often become a critical factor for their installation in the small spaces of oil production platforms. The general objective of the present work is to verify efficiency gains with the injection of bubbles in a gravitational separator through a numerical analysis aiming to improve the quality of the produced water. The simulations were performed using the Eulerian-Lagrangian approach and the SST turbulence model available in ANSYS CFX R1 2021. The inlet water flow ranged from 200 to 450 ml/s and the oil flow was 25 ml/s forming a total of 4 numerical cases. Inlet droplet diameter distributions were implemented using the Discrete Diameter Distribution. The validation of this study was based on the estimation of the cut-off diameter of the oil droplets at the water outlet, where the maximum error was 18.12% in relation to the experimental data. The injection of bubbles in the gravitational separator reduced by up to 22% the cut-off diameter of the oil droplets at the water outlet. It was then concluded that bubble injection can be beneficial for phase separation, especially at higher flow rates.*

Keywords: *gravitational separator, numerical analysis, Eulerian-Lagrangian, bubble injection*

1. INTRODUCTION

In a typical oil reservoir, oil, natural gas and water are found (Silva et., al 2007). The mixture is transferred to a primary processing plant, which consists of a set of equipment with the purpose of separating the phases, either for commercial purposes (oil and gas) or for disposal (water). Generally, the gravity separator is the first and largest processing equipment in a primary processing plant. After the initial gravitational separator treatment, the produced water is sent to the hydrocyclone treatment, where much of the oil is removed. However, it still does not meet the environmental legislation for its disposal, CONAMA resolution nº 393/07, which determines a maximum concentration of 29 ppm of oil. Due to this, it is necessary to use flotators for the fine treatment of the water, which will later be discarded.

Experimental studies involving gravitational separators are difficult and expensive. Even on a small scale, experimental gravity separators are large pieces of equipment that require a complex test circuit, consisting of hydraulic pumps, a set of valves, among other components (Simmons and Azzopardi, 2000; Simmons et al. 2002). Numerical simulation is a low-cost alternative means that can be used to simulate real flows. Furthermore, it can simulate flow conditions not reproducible in experimental tests and provide more detailed information about phenomena involved in phase separation. Therefore, properly validated numerical simulations can be used as design and optimization tools for these equipment.

Several experimental and numerical studies using CFD (Computational Fluid Dynamics) were carried out to evaluate the influence of parameters such as droplet size distribution, continuous and dispersed phase flow rates, mixing velocity and retention time in phase separation (Simmons and Azzopardi, 2000; Laleh et al., 2012; Kharoua et al., 2013; Abdulkadir and Hernandez-Perez, 2010).

Aiming at the development of more efficient and compact equipment for the separation of phases (water, oil and gas), in the present work a numerical study was carried out evaluating efficiency gains through the injection of bubbles in a gravitational separator. The simulations were performed in the commercial software ANSYS CFX R1 2021, using the Eulerian-Lagrangian approach.

2. EXPERIMENTAL METHODOLOGY

The experimental data used for the validation of this study were obtained through an experimental circuit composed of a horizontal gravitational separator fed with a water-oil mixture. The oil used was white mineral oil (with density from 838 to 854 kg/m³ at 20 ºC and viscosity from 14.2 to 17 cst at 40 ºC).

2.1 Experimental circuit

The experiments were carried out in an experimental circuit consisting of a water supply line and an oil supply line capable of supplying water and oil under controlled conditions to the gravitational separator. The experimental circuit is shown schematically in Fig. 1.

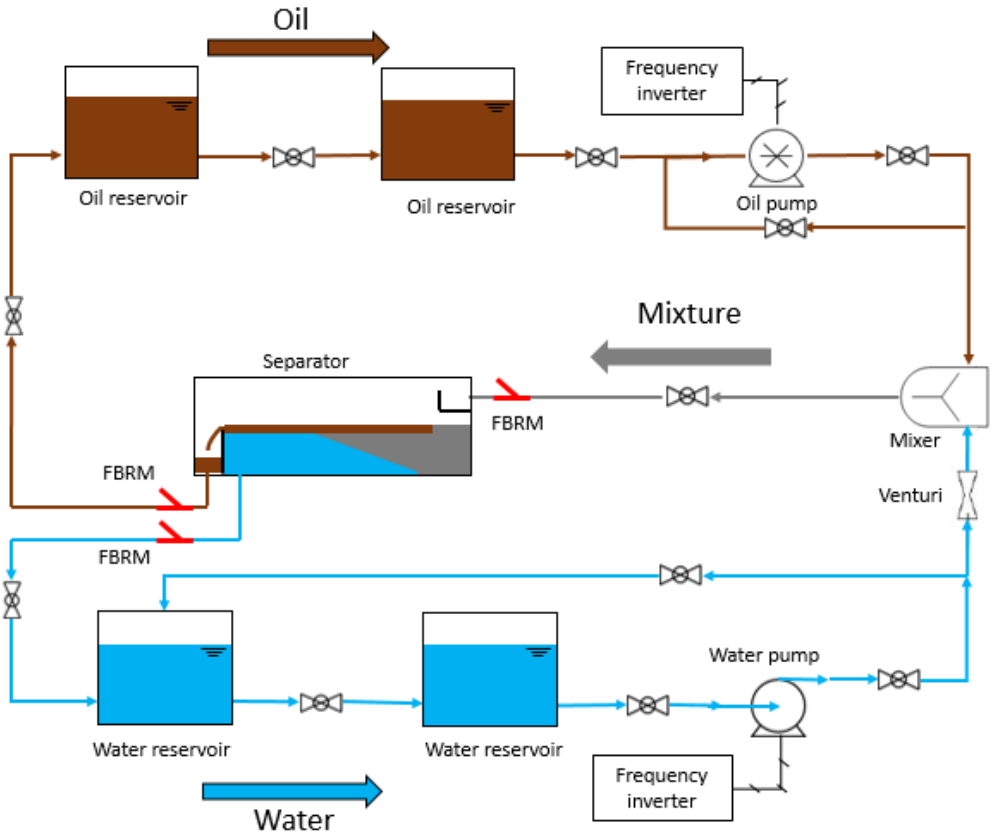

Figure 1. Simplified schematic representation of the experimental circuit.

The water supply line consists of two reservoirs with a capacity of 50 liters. For water circulation, a centrifugal pump was used, model Dancor Cam-W10 1.5CV Three-phase 220/380V with a maximum flow of 1.5 m³/h, powered by a frequency inverter for controlling the volumetric flow rate. The water flow was monitored through a Venturi flow meter and a pressure transducer right at the pump outlet. To calibrate the pressure difference, a Coriolis Yokogawa® flow meter (RCCT38) was used, which has a measurement uncertainty of 0.1%.

The oil supply line consists of two reservoirs with a capacity of 50 liters. For oil circulation, an external gear pump, model FB FBE 3/4" Standard, was used, powered by a frequency inverter for controlling the volumetric flow rate. In volumetric pumps, the flow has a linear behavior in relation to rotation, which made it possible to measure the flow only with the pump frequency, which can vary from 0Hz to 60Hz.

2.2 Measurement of droplet diameters

Droplet diameters were obtained using a FBRM (Focused beam reflectance measurement) sensor. This sensor consists of a probe with a laser beam and a receiver, as shown schematically in Fig. 2.

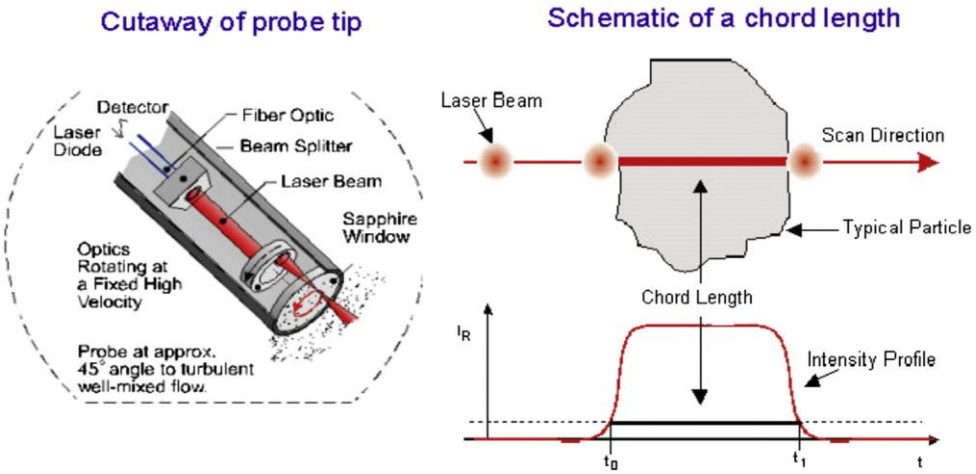

Figure 2. FBRM chord length measurement.
Available from: Clain, 2015.

The probe directs a laser into the fluid which rotates so that the scan path is a small circle. The probe measures the amount of light that is reflected by the fluid and the particles it contains. When the laser moving along the scanning path crosses a particle or droplet, the intensity of the reflected light changes. From the rotation speed of the laser and the reflection time, the distance swept in the particle, known as the string length or drop string, is determined. Generally, several particles per second are measured, providing a distribution of particle sizes (Clain, 2015).

3. MATHEMATICAL AND NUMERICAL MODELING

The simulations were performed in the commercial software ANSYS CFX R1 2021, using the multiphase Eulerian model in steady state as a starting point for the Lagrangian Particle Tracking. Therefore, the approach adopted in the present study was the Eulerian-Lagrangian approach.

3.1 Governing equations

In the Euler-Euler formulation, the transport equations are solved separately for each phase. The conservation of mass and momentum equations for incompressible and isothermal flow for a phase *q* are given by (ANSYS, 2015):

$$\frac{\partial}{\partial t}(\alpha_q \rho_q) + \nabla \cdot (\alpha_q \rho_q \vec{u}_q) = 0 \tag{1}$$

$$\frac{\partial(\alpha_q \rho_q \vec{u}_q)}{\partial t} + \nabla \cdot (\alpha_q \rho_q \vec{u}_q \vec{u}_q) = -\nabla(\alpha_q p_q) + \nabla \cdot (\alpha_q \vec{\mathrm{T}}_q) + \alpha_q \rho_q \vec{g} + \vec{M}_q \tag{2}$$

with a constraint condition:

$$\sum \alpha_q = 1 \tag{3}$$

where $\alpha_q, \rho_q, \vec{T}_q$ and u_q, are the volume fraction, density, Reynolds stress tensor and velocity for a phase *q*.

3.2 Interfacial forces

The total force on phase *q* due to interaction with other phases is denoted $\vec{M}_q$. Considering only the drag and lift interfacial forces can be expressed as:

$$\vec{M}_q = \vec{F}_{D,q} + \vec{F}_{L,q} \tag{4}$$

The drag force ($\vec{F}_{D,q}$) can be respectively formulated as:

$$\vec{F}_{D,q} = \frac{C_D}{8} A_{qp} \rho_q \left|\vec{u}_p - \vec{u}_q\right| (\vec{u}_p - \vec{u}_q) \tag{5}$$

where A_{qp} is the interfacial area density. The drag coefficient, C_D is calculated by the Schiller-Naumann model:

$$C_D = \begin{cases} 24(1+0{,}15\,\mathrm{Re}^{0{,}687})/\mathrm{Re} & \mathrm{Re} \le 1000 \\ 0{,}44 & \mathrm{Re} \ge 1000 \end{cases} \tag{6}$$

The lift force ($\vec{F}_{L,q}$) can be respectively formulated as:

$$\vec{F}_{L,q} = C_L \rho_p \alpha_q (\vec{u}_q - \vec{u}_p) \times (\nabla \times \vec{u}_q) \tag{7}$$

There are several models for calculating the lift coefficient, but in this work the default value of ANSYS CFX was used, where $C_L = 0{,}5$.

3.3 Lagrangian Particle Tracking

The total particle phase flow is modeled by tracking a small number of particles through a continuous phase. The particles can be solid particles, drops or bubbles. The application of Lagrangian tracking in CFX involves the integration of particle trajectories through the discretized domain. As each particle is tracked from its injection point to its final destination, the tracking procedure is applicable to steady-state flow analysis. Particle displacement is calculated using direct Euler integration of particle velocity over time step (ANSYS, 2015). As $(dx_p / dt) = u_p$, the displacement of the particle is given by:

$$x_p^n = x_p^o + u_p^o \delta t \tag{8}$$

The superscripts *o* and *n* refer to old and new values of each property, respectively, and u_p^o is the initial velocity of the particle. In direct integration, it is assumed that the particle velocity calculated at the beginning of the time step prevails over the entire step. At the end of the time step, the new particle velocity is calculated using the analytical solution to the particle momentum equation:

$$m_P \frac{du_p}{dt} = F_D + F_E \tag{9}$$

The drag force on a particle is proportional to the slip velocity between the particle and the fluid velocity. For an oil droplet or a gas bubble dispersed in a continuous phase of water, the drag force can be defined as:

$$F_{D,FP} = \frac{1}{2} C_{D,FP} \rho_F A_{FP} \left|\vec{u}_F - \vec{u}_P\right| (\vec{u}_F - \vec{u}_P) \tag{10}$$

where the drag coefficient is calculated by the Schiller-Naumann model.

The buoyant force is the force acting on a particle immersed in a fluid. For an immersed oil drop or gas bubble, the buoyant force is given by:

$$F_{E,FP} = \frac{\pi}{6} {d_P}^3 (\rho_P - \rho_F) \vec{g} \tag{11}$$

where d_P is the diameter of the droplet.

3.4 Turbulence model

Currently, the most used turbulence models are those of two transport equations. The most common two-equation models are: standard *k-ε* Model, Wilcox's *k-ω* Model, and the *k-ω* Shear Stress Transport (SST).

In the present work, turbulence modeling will be performed using the *k-ω* Shear Stress Transport (SST) model, which is basically a combination of the standard *k-ε* and Wilcox *k-ω* turbulence models. The equations in the SST model are expressed as:

$$\frac{\partial k}{\partial t}+\frac{\partial (u_i k)}{\partial x_i}=\frac{\partial}{\partial x_i}\left[\left(\nu+\frac{\nu_t}{\sigma_{k3}}\right)\frac{\partial k}{\partial x_i}\right]+P_k-\beta^* k\omega \tag{12}$$

$$\frac{\partial \omega}{\partial t}+\frac{\partial (u_i \omega)}{\partial x_i}=\frac{\partial}{\partial x_i}\left[\left(\nu+\frac{\nu_t}{\sigma_{\omega 2}}\right)\frac{\partial \omega}{\partial x_i}\right]+\alpha_2\frac{\omega}{k}P_k-\beta_2\omega^2+2\frac{1}{\sigma_{\omega 2}\omega}\frac{\partial k}{\partial x_i}\frac{\partial \omega}{\partial x_i} \tag{13}$$

where the closure coefficients are the terms: β_3, α_3, σ_{k3} and $\sigma_{\omega 3}$. The coefficient values are changed according to the *k-ε* or *k-ω* model.

3.5 Geometry and mesh

Due to the symmetry of the gravitational separator and the advantages that the geometric division provides, only half of the separator was modeled, as shown in Fig. 3.

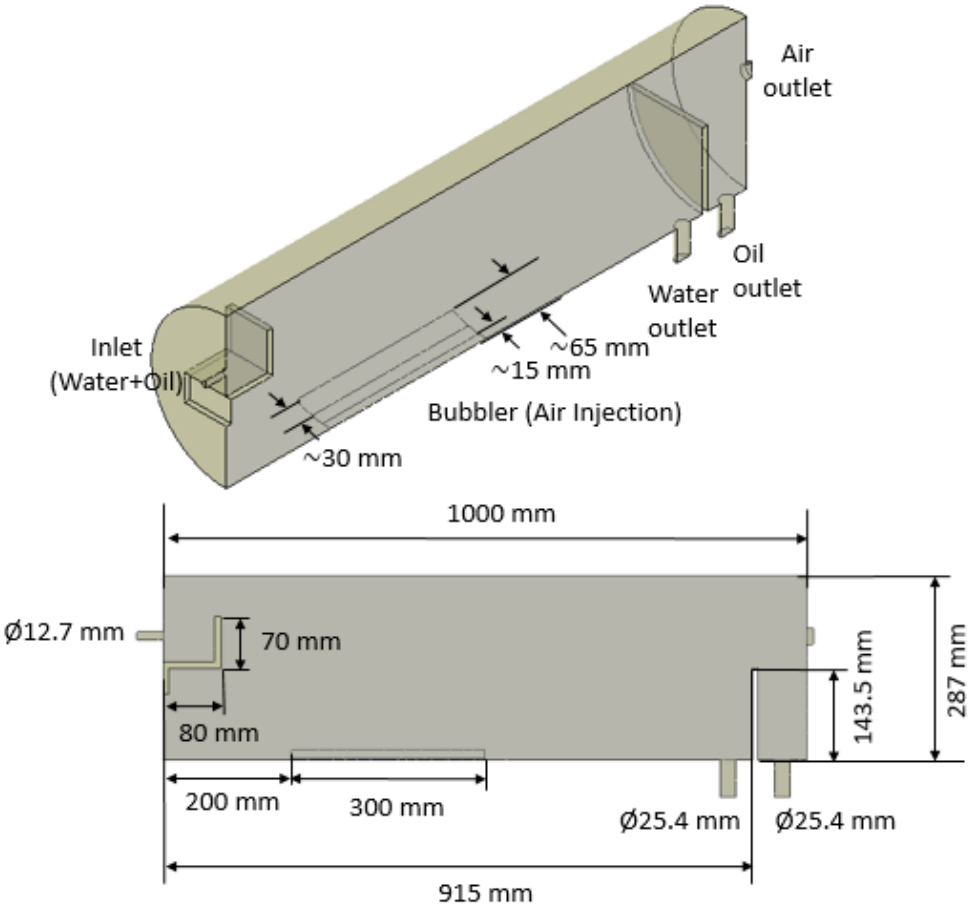

Figure 3. 3D geometry of the gravitational separator half.

For the preliminary study, a tetrahedral mesh was developed in ANSYS ICEM CFD called mesh M1 (Fig. 4). The mesh M1 was refined in some regions of the gravitational separator: inlet and outlets; on the deflector plate; in the air injection (Bubbler) region; near the interfaces; and in the plate of water weir.

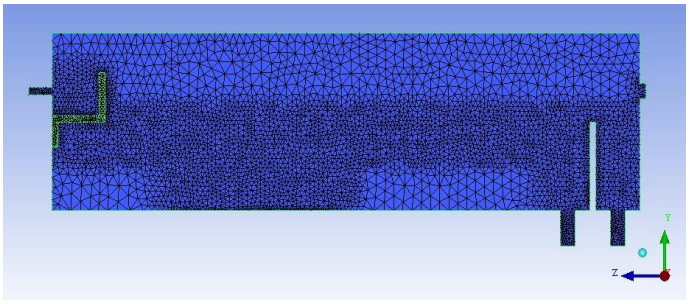

Figure 4. M1 tetrahedral mesh.

The inlet, outlets and bubbler have been refined due to the higher flow velocity in these regions. The baffle plate region was refined due to the impact and change of direction that the liquid mixture undergoes when entering the separator. The proximities of the interfaces were refined due to the interactions between the water-oil and oil-air phases. The plate of water weir region was refined by the fact that it separates the phases present inside the separator.

From coarse mesh M1 another three meshes were generated reducing the Global Element Scale Factor of ICEM CFD: medium mesh M2, fine mesh M3 and large mesh M4. The characteristics of each mesh are presented in Tab. 1.

Table 1. Characteristics of the generated meshes.

Mesh	Number of Elements	y^+	h_W	Dev. %	$\dot{m}_{W\_OW}$	Dev. %	Comp. Time
M1	681,559	8.10	0.1063	0.18	-0.1251	0.51	12h28m
M2	1,045,044	7.24	0.1057	0.21	-0.1276	0.26	17h28m
M3	1,589,998	5.52	0.1063	0.18	-0.1281	0.21	18h25m
M4	2,205,479	4.77	0.1081	0	-0.1302	0	26h36m

The results presented refer to the variation of the water level (h_W) and the variation of the water flow at the water outlet ($\dot{m}_{W\_OW}$) for a flow of 250 ml/s of water and 25 ml/s of oil. Note that mesh M3 was the mesh that obtained the best results with a shorter computational time compared to mesh M4. Therefore, the mesh M3 was the mesh used in this study.

3.6 Boundary Conditions and Initial Condition

For the initial simulation in steady state (Eulerian), the mass flow rates and volumetric fractions of the phases were prescribed. The three-phase mixture is assumed water continuous, with the oil and air being considered dispersed phases in the form of spherical droplets and bubbles in the computed flow. The summary of boundary conditions is presented below:

- Inlet
  - Water: Mass flow rate (specified along with a direction component) and volumetric fraction;
  - Oil: Mass flow rate and volumetric fraction;
- Bubbler:
  - Air: Normal speed (the magnitude of the inlet velocity is specified and the direction is taken to be normal to the boundary) and volumetric fraction;
- Outlet:
  - Air: Opening (an opening condition allows the fluid to cross the boundary surface in either direction);
  - Oil: Opening;
  - Water: Static Pressure (constrains the average pressure to a user-specified value);
- Symmetry: Symmetry (imposes constraints that ‘mirror’ the flow on either side of it);
- Wall: No slipping (the velocity of the fluid at the wall boundary is set to zero).

The average diameter of the oil droplets was defined based on the Sauter Mean Diameter, defined by:

$$d_{32} = \frac{\sum n_i d_i^3}{\sum n_i d_i^2} \tag{14}$$

where n_i is the number of drops with diameter d_i.

The Lagrangian tracking of particles is done over an existing flow field, in this case, the Eulerian steady-state simulations performed initially. The boundary conditions used in Lagrangian particle tracking are shown below:

• Input (Oil droplets)
  – Mass flow rate: The same used in the oil phase in the Eulerian simulation;
  – Number of droplets inserted: 10,000 (number defined with a preliminary study that showed that from 10,000 drops the distribution of oil drops in the water outlet is always the same).

The droplet diameter distributions at the inlet were experimentally implemented through the Discrete Diameter Distribution. The initial condition assumes that the gravitational separator already has a 104 mm water column and a 39.5 mm oil cap. Due to possible measurement errors of the FBRM sensor, the experimental cut-off diameter was defined as the diameter of the oil drop that represents 99.865% of the oil droplets in the water outlet. In the numerical model, the cut-off diameter was defined as the largest drop of oil present in the water outlet.

3.7 Computational conditions

The numerical parameters used in this study are presented in Tab. 2. They were defined based on similar works (Vilagines and Akhras, 2010; Torriano et al., 2017) and on the recommendations of the Ansys CFX Theory Guide.

Table 2. Summary of numerical parameters used in this study.

Multiphase Approach	Turbulence Model	Approximation of the advective term	Approaching the interface	Convergence Criterion	Lagrangian Particle Tracking
Eulerian-Lagrangian	SST	*High Resolution*	Compression scheme ($k_{comp} = 2$)	RMSE 10^{-4}	*One-way-coupling*

4. NUMERICAL RESULTS

Table 3 presents the test grid developed based on the experimental tests performed in the gravitational separator.

Table 3. Average flow rates of water and oil measured experimentally.

Cases	Oil flow [ml/s]	Water flow [ml/s]
Case 1	25	211
Case 2	25	250
Case 3	25	350
Case 4	25	450

4.1. Distribution of oil droplet diameters at the inlet

The droplet size distribution data obtained experimentally were implemented in the numerical model. The distributions generated for cases 1, 2, 3 and 4 are shown in Fig. 5.

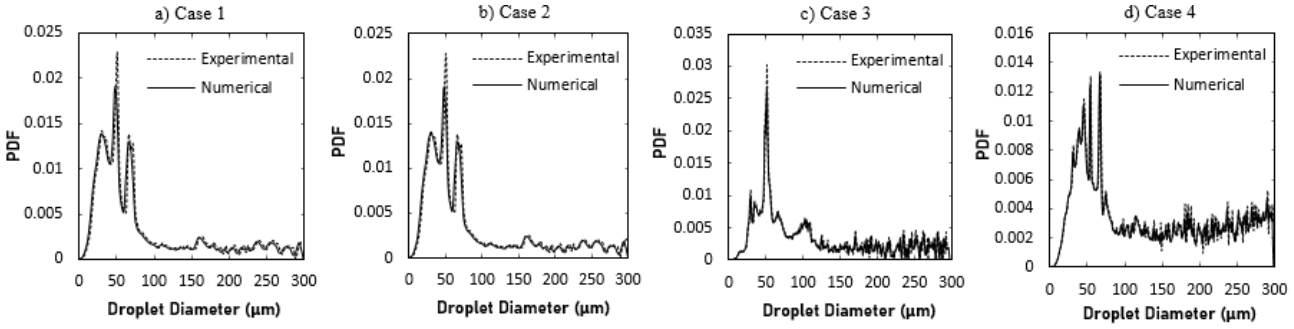

Figure 5. Distribution of droplet diameters at the inlet.

For case 1, the average percentage error was 11.25% in relation to the experimental PDF and standard deviation was 11.33. For case 2, the average percentage error was 16% in relation to experimental PDF and the standard deviation was 16.7. For case 3, the average percentage error was 23.73% in relation to experimental PDF and the standard deviation was 38.20. For case 4, the discrete distribution, the average percentage error was 11.01% in relation to the experimental PDF and the standard deviation was 11.85.

4.2. Validation and Analysis with air bubble injection.

Initially, 10,000 iterations were performed with the mass flow of water at the inlet equal to the mass flow of water at the outlet water to obtain an estimate of the static pressure at the outlet water. The pressure at which the water level remained relatively constant at approximately 104 mm was: 1725 Pa for case 1, 1668 Pa for case 2, 1480 Pa for case 3 and 1247 Pa for case 4. The liquid level variation using the estimated pressure is shown in Fig. 6 and the average water level for the last 5000 iterations is shown in Tab. 4.

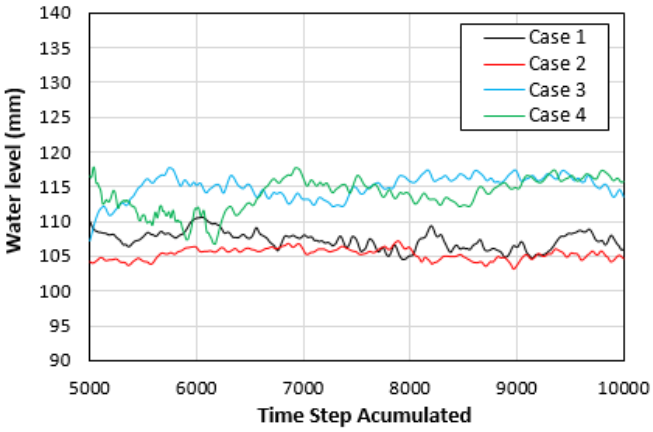

Figure 6. Water level variation in the last 5000 iterations.

Table 4. Average water level numerical for the last 5000 iterations.

	Experimental	Case 1	Case 2	Case 3	Case 4
Average water level	~104 mm	107.3 mm	105.3 mm	115 mm	113.9 mm

The greater the flow of water at the inlet, the more difficult it is to stabilize the liquid level inside the separator. This is clear in the departure of the water level in relation to the experimental data with the increase of the water flow.

The results found for case 1, case 2, case 3 and case 4 are illustrated in Fig. 7, through the density gradient inside the gravitational separator and the oil droplet trajectories.

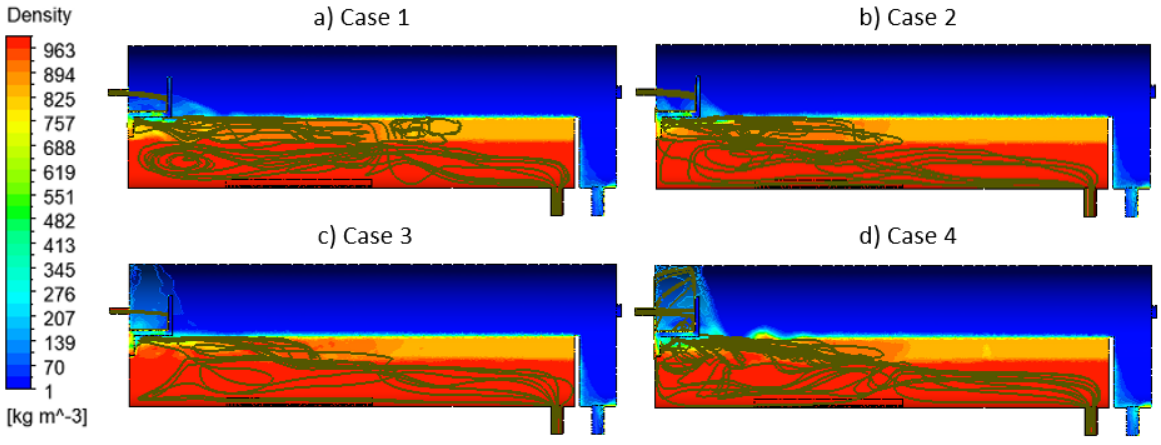

Figure 7. Density gradient and oil droplet trajectories in the gravitational separator.

The oil droplet diameter distributions obtained at the water outlet are shown in Fig. 8. There is a good agreement between the numerical data and the experimental data for cases 1 and 2. As for the cases 3 and 4, there is a greater divergence in relation to the experimental data.

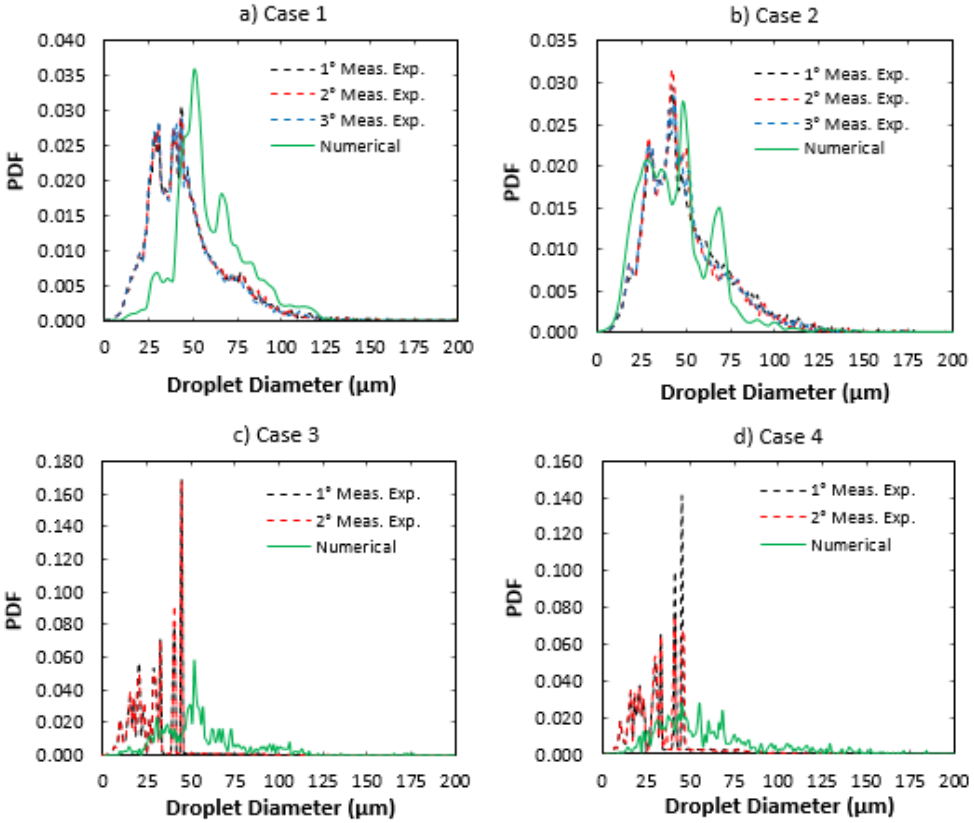

Figure 8. Distribution of oil droplet diameters in the water outlet.

The validation of the numerical model was performed by comparing the data on the cut-off diameter of the oil droplets at the water outlet obtained numerically with the data obtained experimentally, as shown in Fig. 9.

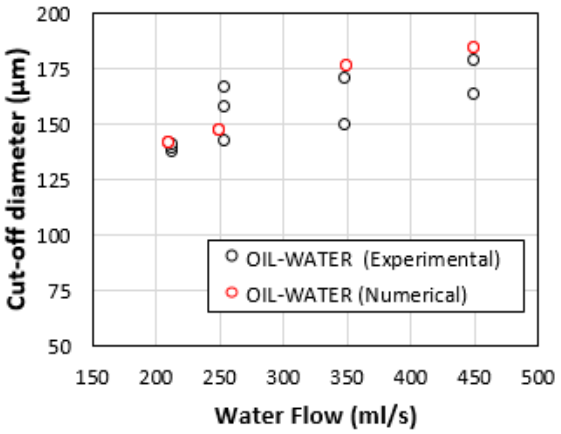

Figure 9. Experimental cut-off diameter x Numerical cut-off diameter.

The maximum relative error in relation to the experimental data was 2.92% for case 1, 11.45% for case 2, 18.12% for case 3 and 12.88% for case 4. The numerical results obtained have a good agreement with the experimental results, therefore, the numerical model is validated.

After validation of the numerical study, the flow analysis was performed with the injection of air bubbles with an average diameter of 100 µm and injection velocity of $1x10^{-5}$ m/s. The results found for the cut-off diameter of the oil droplets at the water outlet are shown in Fig. 10.

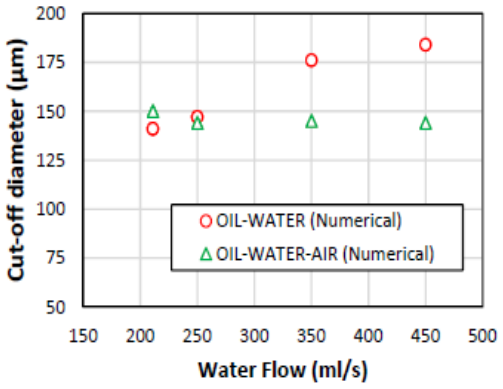

Figure 10. Comparison of the cut-off diameter with and without air bubble injection.

It is observed that the greater the flow of water at the inlet, the greater the cut-off diameter, as expected. The case with the lowest water flow at the inlet (case 1) was the only case where the injection of air bubbles increased the cut-off diameter. This is due to the fact that the injection of air increases the turbulence in the flow, which causes an increase in the drag of the oil droplets. For the other cases of the test grid, the injection of air bubbles was beneficial for the phase separation. Cases 3 and 4 had the greatest reduction in cut-off diameter with air bubble injection, 18% and 22%.

5. CONCLUSION

From the results presented in this work, it was possible to conclude that the numerical model is able to reproduce the physics and the trend of the behavior observed experimentally, with a maximum error of 18.12% in the cut-off diameter.

The injection of air bubbles reduced the cut-off diameter by up to 22%, which means a considerable reduction in the diameters of the oil droplets at the water outlet, which leads to an increase in the efficiency of the equipment. It can be concluded that the injection of air bubbles can allow the development of a more efficient and compact equipment.

6. REFERENCES

Abdulkadir, M., Hernandez-Perez, V. The effect of mixture velocity and droplet diameter on oil-water separator using computational fluid dynamics (CFD). *World Academy of Science, Engineering and Technology*, p. 44-51, 2010.

ANSYS, Inc. ANSYS-CFX® – SOLVER THEORY GUIDE, 2015.

Clain, P. Particle size distribution of TBPB hydrates by focused beam reflectance measurement (FBRM) for secondary refrigeration application. *International Journal of Refrigeration*, v. 50, n. 0, p. 19–31, 2015.

Kharoua, N., Khezzar, L., Saadawi, H. CFD modelling of a horizontal three-phase separator: a population balance approach. *American Journal of Fluid Dynamics*, v. 3, n. 4, p. 101-118, 2013.

Laleh, A.P., Svrcek, W.Y., Monnery, W.D. Design criteria for oilfield separators improved by computational fluid dynamics. *Chemical Engineering and Technology*, 35, No. 2, p. 323–333, 2012.

Silva, A.L.F. et al., Processamento Primário de Petróleo - Petróleo Brasileiro S.A. Rio de Janeiro, Brasil, 2007.

Simmons, M. J. H., Wilson, J. A., Azzopardi, B. J. Interpretation of the flow characteristics of a primary oil-water separator from the residence time distribution. *Chemical Engineering Research and Design*, v. 80, p. 471-481, 2002.

Simmons, M. J.H., Azzopardi, B. J. Drop size distributions in dispersed liquid–liquid pipe flow. *International Journal of Multiphase Flow*, 27(5), p. 843–859 2001.

Torriano, F., Lessard, M.C., Thibeault, N. Numerical study of an oil–water flow in a gravitational separator. *International Journal of Computational Methods and Experimental Measurements*, v.6. 326-333, 2017.

Vilagines, R., Akhras, A.R. Three-phase flows simulation for improving design of gravity separation vessels. *SPE Annual Technical Conference and Exhibition. Society of Petroleum Engineers*, 2010.

7. RESPONSIBILITY NOTICE

The authors are the only responsible for the printed material included in this paper.